IEEE Transactions on Automation Science and Engineering (T-ASE) paper, presented at ICRA 2026, Vienna, Austria.
Cite as T-ASE paper.

Modular Acoustic Graph SLAM for Underwater Monitoring With Autonomous Underwater Vehicles

Marta Real, Pau Vial, Roger Pi, Narcís Palomeras, *Member, IEEE*, and Marc Carreras, *Member, IEEE*

***Abstract*—This work was developed under the need for an acoustic localization system to monitor marine protected areas (MPAs) with the help of autonomous underwater vehicles (AUVs). Although the use of acoustic signals for underwater localization has been previously studied, most of the solutions rely on filter-based optimization, which is prone to linearization problems in long-term applications. Instead, we implemented a Modular Acoustic Graph Simultaneous Localization and Mapping (SLAM) algorithm that, using a factor graph framework, tracks acoustic beacons with either ranges or bearings. In addition, we developed several novel methods, like a delayed-position update for ultra-short baseline (USBL) position factor integration process, an initialization algorithm for acoustic landmarks, and the creation of a new 3D bearing factor that combines two angles. After developing the algorithm, field experiments were carried out in different areas on the coast of Catalonia. Besides the localization, some monitoring tasks were also tested, such as visual mapping of localized landmarks or optical transmission of data with seafloor stations, which helped validate the accuracy of the acoustic localization system. The results of such experiments are presented and discussed.**

***Note to Practitioners*—Autonomous robots can benefit underwater monitoring of deep areas. Our work presents a direct application of such robots, which use acoustic signals to localize underwater elements, like monitoring stations in the seafloor equipped with acoustic modems, and interact with them. The navigation is computed using a graph-based approach and can use either range or bearing information for the acoustic localization. The experiments in real scenarios are executed using preplanned trajectories, and the results prove that this system is able to localize acoustic targets within low uncertainty. The next step would be the implementation of path-planning strategies to optimize the localization process.**

***Index Terms*—Autonomous underwater vehicles, simultaneous localization and mapping, factor graphs, acoustic localization, USBL, underwater monitoring.**

I. Introduction

RECENTLY, the United Nations accorded that 30% of the ocean should be protected by 2030 [1]. Nowadays, in Europe, only 12.30% of its marine territory represents MPAs [2]. The creation of new MPAs needs to be accompanied by new technologies and techniques to monitor and manage these areas. One of the available options are fixed marine observatories placed in these areas that gather information such as images, salinity, or temperature. Although this is a useful technology, more versatile and less impacting approaches can be taken. That is the case of the PLOME project (*Platform for Long-lasting Observation of Marine Ecosystems*) [3], which combines easy-to-move stations deployed without cables, named landers, and AUVs (Fig. 1) that help gather more information by extending the operational area further from the stations and also retrieving data to the surface. With these technologies, a modular platform for monitoring the environment in real time can be deployed in different locations when needed. Another project related to monitoring MPAs is BITER-AUV (*A joint effort between BIology and TEchnology to monitor and recover fishery-impacted species and ecosystems: adaptive autonomous vehicles*),[1] which aims to study the behaviour of various benthic species within MPAs on the coast of Catalonia. With this objective, captured fauna is tagged with acoustic beacons and released again in the MPA. Usually, this task is done by detecting the presence of tagged fauna in an MPA using an array of hydrophones over a period of time [4]. Instead, this work applies a fine-scale spatial tracking approach. The AUV will track the animals using the acoustic signals some months after their release to study their movements in the MPA. Both projects share the

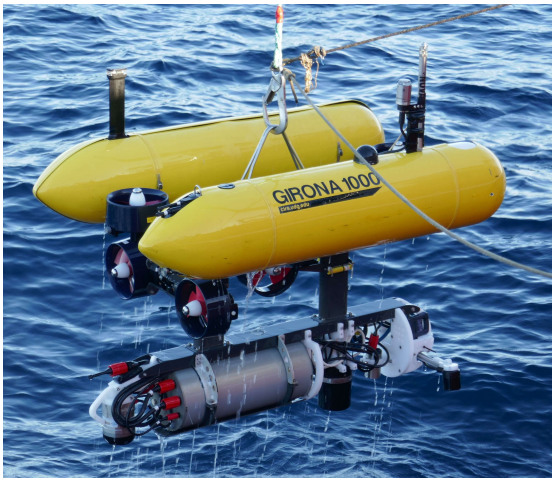

Fig. 1. Girona1000 AUV used in the experiments.

Received 6 March 2025; revised 29 June 2025; accepted 18 September 2025. Date of publication 29 September 2025; date of current version 6 October 2025. This article was recommended for publication by Associate Editor W. He and Editor Z. Li upon evaluation of the reviewers' comments. This work was supported in part by the BITER-AUV Project under Grant PID2020-114732RB-C33 and in part by the Platform for Long-lasting Observation of Marine Ecosystems (PLOME) Project under Grant PLEC2021-007525. *(Corresponding author: Marta Real.)*

The authors are with the Institut VICOROB, Universitat de Girona, Girona, 17003 Catalonia, Spain (e-mail: marta.real@udg.edu).

Digital Object Identifier 10.1109/TASE.2025.3615829

[1] https://cirs.udg.edu/portfolio_page/biter-auv/

need for a reliable acoustic localization and tracking system, either to locate the landers to fix the AUV position and allow more repeatability to survey the area or to track the tagged fauna.

In this context, we present the implementation of a modular acoustic SLAM algorithm based on a factor graph framework that aims to map deployed acoustic landmarks using an AUV and to provide a precise underwater acoustic localization system.

A graph SLAM integrates information from the sensors of the AUV as factors, used as constraints, and estimates both the AUV's poses and the landmarks' positions by applying least squares optimization. In our proposal, the algorithm uses information from both proprioceptive sensors, like a pressure sensor, the velocity measured from a doppler velocity log (DVL), and inertial information from an inertial measurement unit (IMU); and exteroceptive ones, such as estimated positions from the surface vessel using an USBL, and acoustic information from different acoustic beacons on the sea floor (landers or tagged animals) that act as landmarks. In this case, the construction and optimization of the factor graph uses two open-source libraries: the Georgia Tech Smoothing and Mapping (GTSAM) library [5] and the iSAM2 library [6].

The information sent from these landmarks depends on the beacons used in the experiment: the landers from the PLOME project provide ranges via medium-frequency (MF) modems installed in them; instead, the acoustic beacon used to simulate tagged fauna in the BITER-AUV project is a high-frequency (HF) modem that provides two bearings (azimuth and elevation) to the AUV thanks to a HF USBL installed on it.

In our previous work [7], an initial version of a range-based Graph SLAM algorithm was presented. In that work, we tested some parameters and trajectories in a controlled scenario in shallow waters. This current work presents an improved and amplified version of that algorithm alongside successful tests in real deep scenarios.

One relevant improvement is a new initialization method that, by taking into account the uncertainty of an initial landmark estimation, integrates its information to the graph SLAM once it has reduced that uncertainty below a threshold value. This method can be applied to any factor that provides information from a landmark to avoid heavy increases in uncertainty in the graph.

In order to work with bearings in a 3D space, we have also implemented and tested a novel 3D bearing factor to add this information to the factor graph SLAM since the GTSAM library does not include a factor able to combine two angles.

Moreover, a new addition with respect to the previously proposed algorithm is the inclusion of a USBL position factor. This factor adds an approximate position of the AUV by using the security communication between the AUV and its support vessel. Since the position's computation using this communication has a delay and is affected by signal loss, our integration method of the USBL position factor takes into account these elements to set the factor in its correspondent node within the graph SLAM.

The final contribution of this work is an algorithm based on the uncertainty value of the acoustic beacons' estimation that allows the robot to execute autonomously tasks such as visual mapping of the detected landmarks or to act as a "data mule" transferring data from the seafloor stations up to the surface.

Overall, these contributions result in the implementation of a novel underwater factor graph SLAM that can be adapted to many applications thanks to its modularity and the demonstration of its effectiveness in real scenarios in combination with other tasks.

II. Related Work

A. Acoustic Localization and Tracking

Acoustic signals for underwater navigation have been broadly applied as a substitute for global positioning systems based on electromagnetic signals. Their uses encompass a wide range of applications and approaches, like the self-localization of the AUV in an unknown map (estimate where the robot is within such map) or tracking acoustic landmarks (estimate and find other elements in the map). As for self-localization, systems with acoustic beacons in known positions are commonly used, such as long baseline (LBL), short baseline (SBL) [8], or USBL [9]. Although LBL deployment and calibration are usually laborious, some approaches, such as the one in [10], simplify these tasks thanks to their self-calibrating acoustic nodes, while still providing good results. In the case of USBL, they can work as a stand-alone localization system [11] or as support for the vehicle's navigation [12].

Sometimes, the robot's position is not obtained directly from the acoustic localization system, and instead, only part of that information is available. That can be because the beacons are in unknown positions or due to data transmission limitations. Usually, this partial information is in the form of range or bearing measurements, which are used as alternative methods to compute the localization. Range-based localization in underwater SLAM is a common approach due to its versatility in computation methods (time-of-arrival (ToA), time-difference-of-arrival (TDoA), etcetera). Many filter-based methods use range information for AUV localization, such as in [13], where they use the time-of-flight (ToF) to compute ranges from two fixed transponders to estimate their robot's position; or in [14], where they use synchronized acoustic signals to calculate the distance from a surface vessel that acts as the reference. This method is also widely applied for tracking targets such as beacon nodes from an underwater wireless sensor network using ToA [15] or TDoA [16]. Likewise, bearing-based localization is also applied in underwater environments using filtering methods, such as for cooperative navigation between multiple AUV using Extended Kalman Filter (EKF) [17] or Particle Filter (PF) [18]. Also, EKF bearing-only localization algorithms have been implemented for tracking static targets [19], [20]. Outside underwater environments, bearings are commonly used by extracting them from visual landmarks in aerial [21] or wheeled [22] robotics.

Concerning environmental monitoring, previous works apply acoustic methods to aid in the tracking of tagged animals, such as [4], from which the BITER-AUV project is

based on. I. Masmitja et al. work presents an initial study to localize the tagged animals and different techniques used, like TDoA. Another example is [23], where they track a moving target, a leopard shark, with acoustic signals and apply a particle filter method to compute its position. Moreover, static seafloor stations have been used as a combination of data gathering and acoustic transponders for AUV navigation. That is the case of [24], where they use the seafloor station as a reference point, similarly as in this work, but applying filter-based methods to estimate the robot navigation.

B. Graph SLAM

In recent years, the implementation of factor graphs in robotics has increased due to its advantages in front of filter-based techniques such as EKF [25] or PF [26], especially applied to SLAM. The main disadvantage of filter-based SLAM algorithms is that they only compute the last state of the robot, and although they are very efficient computationally, the estimation deteriorates with long-term applications [27] due to error accumulation in the linearization. Instead, factor graph SLAM computes the whole trajectory of the robot at each update without loss of information by treating SLAM as an optimization problem [28]. The problem with this method is that, as the SLAM progresses, the graph increments in size and complexity. Some solvers address this problem by focusing the optimization on the parts of the graph that are affected by the update, which is the case of iSAM [29] and iSAM2.

Pose-graph SLAM is a variation of factor graph SLAM, which estimates only the robot poses during the navigation, and landmarks are used as another set of constraints rather than being part of the solution of the graph. Many applications use this method for SLAM, either in underwater scenarios [30] or other applications [31], [32]. In the sense of a full graph SLAM that estimates the robot poses while mapping the landmarks' positions, in [33] they use a visual graph SLAM to identify and map Aruco markers in a warehouse to localize an uncrewed aerial vehicle (UAV).

Referring to the integration of USBL measurements in a graph, in [34], they implement an underwater pose-graph SLAM that uses a USBL position factor that considers the delay between the transmission of the information and the robot's pose. To achieve that, they find the node with the closest pose to the USBL position data using the absolute time of the nodes. While it avoids adding new nodes and incrementing the size of the graph, it adds an extra step to decide to which node associate the USBL position factor and it is only an approximate position. Another approach, presented in [35], integrates the USBL measurements of slant range and bearings into their preintegrated deadreackoning factor.

Recent works have already applied ranges to pose-graph SLAM, such as [36], where they use a beacon in a pre-known position to close the loop in the navigation of an indoor robot. Similarly, [37] presented a range-based localization algorithm for cooperative navigation. In the case of angle-based factor graph applications, a good example is [38], where they test a combination of EKF and factor graphs with static sensors to estimate the position of anonymous targets. Apropos of full graph SLAM, as far as we are concerned, there are no other applications in underwater scenarios using range or 3D bearings for mapping acoustic landmarks while executing other tasks.

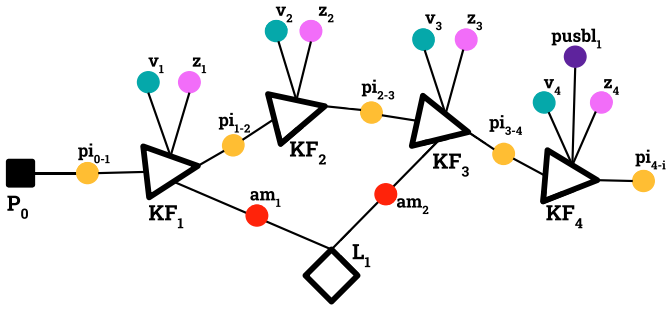

Fig. 2. Factor graph SLAM schematic.

III. Graph SLAM Algorithm

A. Preliminaries

Factor graphs are probabilistic graphical models that use non-linear least squares optimization to estimate the states of the graph nodes. When applied to a SLAM problem, the graph treats robot poses (RP) and landmark poses (L) as the nodes and measurements from the sensors as constraints. These constraints, called factors $\psi_i(rp_j, y_k)$, establish a relation between the robot pose rp_j and another node y_k, which can be either another pose rp_k or a landmark node l_k. The optimization is formulated as:

$$P^*, L^* = argmin_{RP,L} \sum_i \psi_i(rp_j, y_k). \tag{1}$$

Factors are modeled as the comparison between the expectancy model of the measurement $h(x)$ and the measurement taken from the sensor z, computed as the Mahalanobis distance with the covariance matrix Σ, which represents the uncertainty of the estimation:

$$\psi(rp_j, y_k) = \| h(x) - z \|^2_\Sigma, \tag{2}$$

where

$$\| h(x) - z \|^2_\Sigma = (h(x) - z)^\top \Sigma^{-1} (h(x) - z). \tag{3}$$

For example, in the case of the between factor, which is a binary factor that established the odometry between two poses, the factor is the Mahalanobis distance between the estimated distance from one node to the other and the measured value from the sensors z' plus zero mean Gaussian error η:

$$z = z' + \eta. \tag{4}$$

B. Pose-Graph Framework

The base used to implement this algorithm is a modular inertial pose graph that uses proprioceptive sensors to estimate the dead-reckoning navigation of the robot [39]. It is modular since it can easily integrate external factors from exteroceptive sensors and thus adapt to multiple SLAM problems.

Figure 2 shows the factor graph structure for this application. Its main elements are the key frames of the robot's poses (triangle shapes noted as KF_i in the figure) and the

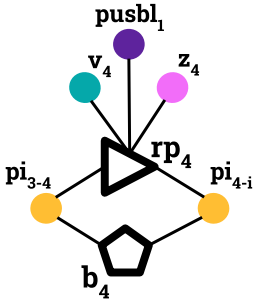

Fig. 3. Key frame example.

nodes corresponding to the landmark estimations (rhomboid noted as L_1). The factors used are preintegrated inertial factors (in yellow noted as pi_{i-j}), USBL position factors from the surface vessel (in purple noted as $pusbl_1$), and acoustic measurement factors (either range or bearings, in red noted as am_i). The green and pink circles correspond, respectively, to the velocity (v_i) and depth (z_i) priors added to each key frame. P_0 represents the prior state to which the graph is anchored.

These key frames are composed of two nodes, one for the robot's pose and the other with the sensors' bias. All the factors connected to a key frame connect with the robot's pose node (noted as rp_i), and the sensor bias node (noted as b_i), which is only connected to the preintegrated inertial factors, since it only considers the proprioceptive sensors of the robot. This is shown in the example for key frame 4 in Figure 3. Each time an exteroceptive sensor has a new measurement, the graph adds a new key frame, updates the state's estimation, and starts the inertial preintegration again. The preintegration is the composition of the measurements provided by the IMU during a period of time. Once a new key frame is created, the previous preintegration computation stops and builds the preintegrated inertial factor [40], which contains the pose increment between two key frames of the graph in the SE (3) group. Besides the preintegrated inertial factor, two prior factors with the last information of the DVL (linear velocity) and the pressure sensor (depth) are added to the robot's pose node. In addition, to avoid a large accumulation of measurements in the preintegration, a new key frame is set periodically in case too much time has passed from the latest node update (KF_2 in Fig. 2 for example). In terms of how our navigation system with the graph SLAM algorithm works, Figure 4 shows its logical sequence.

C. Usbl Position Factor

During the mission, the AUV communicates with the surface vessel via bidirectional acoustic signals between a medium-frequency modem installed at the top of the robot and a USBL in the support boat. This acoustic communication transmits information to the AUV (for example, missions or orders) and receives the robot's general state for monitoring. By using the transmission time of the acoustic signal from the robot to the boat's USBL and the global positioning system (GPS) position of the boat, the USBL also computes an estimated position of the robot. This estimated position is then sent back to the AUV. Since the information provided by the boat's USBL is a 3D point in the GPS frame, first, it needs to be transformed into the world NED frame. Then, the translation between the communication modem position and the robot's frame is added before integrating the USBL position factor into the graph SLAM. Therefore the observation model z'_{usbl} becomes:

$$z'_{usbl} = {}^{w}P_r = {}^{w}T_u \oplus {}^{r}t_m, \tag{5}$$

where ${}^{w}T_u$ is the transformation from the boat's USBL pose w.r.t. world NED frame, ${}^{r}t_m$ is the translation of the modem's position with respect to the robot's frame, and ${}^{w}P_r$ is the measured position to be used for the USBL position factor. The expectancy model $h(x)_{usbl}$ corresponds directly to the estimation of the robot's position extracted from the graph SLAM.

Since there is a delay between the estimation and the actual pose of the robot at the moment of receiving the signal back (Figure 5), we created an integration method to address this problem. This delayed-position update method works as explained next: First, when the USBL initiates communication by sending an acknowledgment signal, the graph adds a new node with only the inertial information at that moment, and the index of that node is stored. Then, the AUV sends back a signal to the vessel, which the USBL uses to compute the position of the AUV. Finally, the USBL responds to the AUV with the position information. This estimated position is transformed into the robot's frame and added as a 3D point factor to the node previously created with the stored index. This process is iterative, meaning that when the USBL sends back the position to the AUV, it also acts as an acknowledgment signal, so apart from adding the position to a previously created node, the graph also adds a new node for the following position to be received.

Due to signal losses in underwater acoustic communication and considering the time between transmissions, the algorithm discards the position factors that take longer than a time threshold. For example, considering that the AUV receives information from the vessel every 10 seconds approximately if the time between the acknowledgment signal and the position signal is 20 seconds, this means a signal has been lost in between, so the new position and the node index are discarded. Also, an outlier rejection function discards any USBL measurement that surpasses the maximum distance threshold between the position sent by the USBL and the one from the robot's navigation by computing their Euclidean distance. Although a USBL position could be rejected, the key frame created with only the preintegrated inertial factor is maintained in the graph.

D. Range Factor

The range factor ψ_r is a between factor like Eq. 2 that establishes a fixed distance between the last AUV pose (rp_j) and the position of the measured acoustic landmark (l_k) using the range measurement z'_r. Its observation model is:

$$z'_r = \sqrt{(x_{mod} - x_l)^2 + (y_{mod} - y_l)^2 + (z_{mod} - z_l)^2}, \tag{6}$$

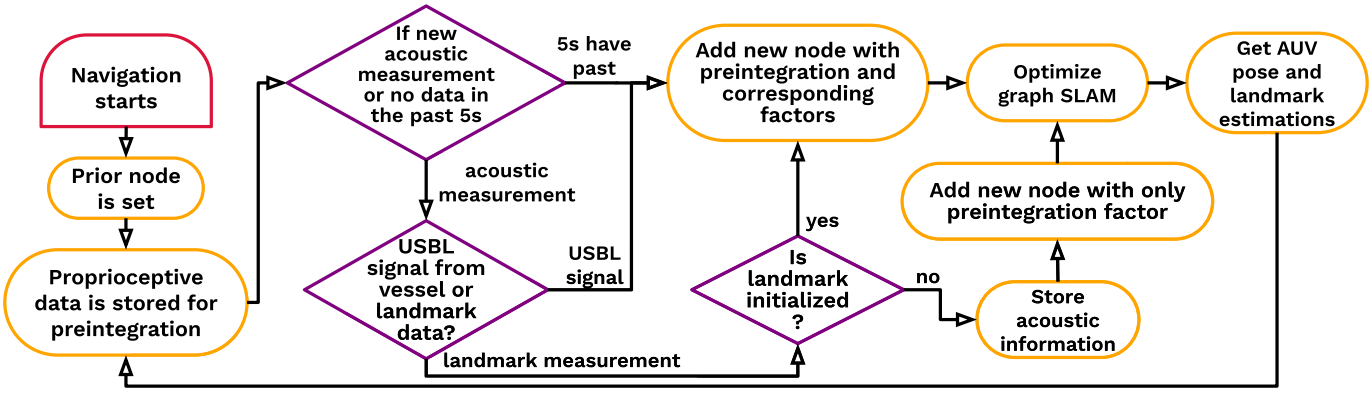

Fig. 4. Simplified version of the acoustic Graph SLAM algorithm.

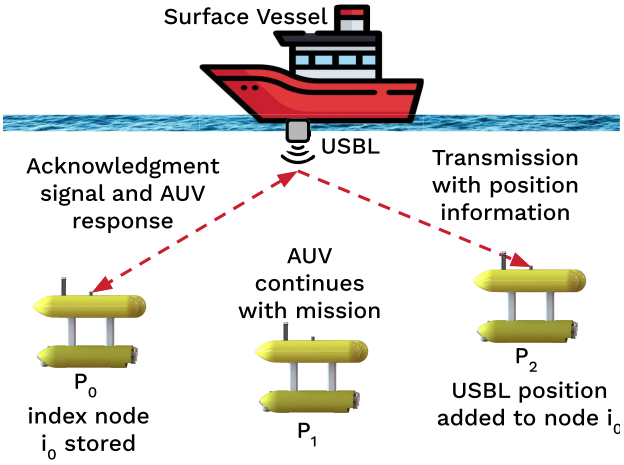

Fig. 5. USBL communication sequence.

where x_{mod}, y_{mod} and z_{mod} are the coordinates of the modem with respect to the world frame and x_l, y_l and z_l are the coordinates of the landmark. The range's expectancy model $h(x)_r$ is the estimated distance between rp_j and l_k computed as the translation between these two points considering the transformations between frames:

$$h(x)_r = |^{mod}P_l| = |{}^r t_{mod}^{-1} \oplus^w t_r^{-1} \oplus^w P_l|, \tag{7}$$

where ${}^r t_{mod}$ and ${}^w t_r$ are the translations from the modem position to the robot frame and from the robot frame to the world frame respectively, and ${}^w P_l$ is the estimated position of the landmark with respect to the world frame. In this case rotations are not considered since they do not affect the range measurements. Thus, the factor ψ_r results in:

$$\psi_r(rp_j, l_k) = \| h(x)_r - (z'_r + \eta_r) \|^2_\Sigma . \tag{8}$$

To integrate this information in the graph, we used the preexisting RangeFactor provided by the GTSAM library [5]. Apart, the zero mean Gaussian noise added to the range factor is modeled as $\eta_r \sim \mathcal{N}(0_{1\times1}, \sigma_r)$, where the standard deviation σ_r was determined empirically and can be checked at Table I in Section IV-A.

As previously mentioned, we presented an early version of this algorithm in [7], where both the factor noise (σ_r) and the robot trajectories were tested. One of the main improvements has been the implementation of a procedure to initialize the acoustic landmarks in the graph. Algorithm 1 shows a general overview of the initialization method. Essentially, the initialization builds a temporal factor graph that only includes two factor types: the acoustic factors from a specific landmark (id_j) with the measurement (am_i), and the odometry between poses (rp_m) where the AUV received the signals. The information for these factors is stored in AM_j and RP_{mj} each time a new measurement is received, and the landmark id_j is not yet initialized. Once the graph is optimized, it computes the estimation of that landmark and its corresponding covariance

TABLE I
MEASUREMENTS' NOISES

Associated measure	Standard deviation	Value
Range	σ_r	0.01 m
Azimuth	σ_a	0.25 °
Elevation	σ_e	0.25 °
USBL position	σ_u	10 m

Algorithm 1 Acoustic Landmark Initialization

Receive acoustic measurement (am_i) with landmark identifier (id_j)
if Landmark id_j not initialized **then**
  $AM_j \leftarrow am_i$
  $RP_{mj} \leftarrow rp_m$
  if AM_j size $\geq$ minimum n° of landmarks **then**
    Build temporal graph with information from AM_j and RP_{mj}
    Optimize temporal graph
    Compute Landmark id_j matrix covariance trace (tr)
    if $tr \leq threshold$ **then**
      Add factors with the stored information in AM_j to main graph
    end if
  end if
  Reset temporal graph
else if Landmark id_j initialized **then**
  Add factor with am_i and id_j to main graph
end if

matrix. The trace of the covariance matrix serves to evaluate the uncertainty of the landmark position. If this uncertainty is below a threshold value, then all the acoustic factors are added to the general graph in their correspondent nodes. This method avoids uncertainty increases in the main graph while the landmark is still non-observable (e.g. the AUV moves in a straight line) or while there are still a small number of measurements and it is more prone to non-convergence. The threshold was set to 100 m^2 for both range and bearing-based SLAM after doing tests in shallow waters, before the deep waters experiments. Once the landmark is added to the main graph, its uncertainty is smaller than the threshold since the main graph has more inertial information and can provide a more accurate estimation.

E. 3D Bearing Factor

The bearing factor represents a vector drawn from the AUV pose to the direction of the acoustic landmark. Two angles compose this vector: the azimuth

$$\theta = atan\left(\frac{y}{x}\right), \tag{9}$$

and the elevation

$$\varphi = atan\left(\frac{z}{\sqrt{x^2+y^2}}\right), \tag{10}$$

thus the raw measurement is $z'_b = [\theta, \varphi]$.

This factor compares the expected vector between the AUV pose and the landmark position (Vec_{est}) and the vector computed through the composition of both measured angles (Vec_{meas}). To do so, we use unitary vectors and calculate the error between them. On the one hand, the vector from the raw measurement Vec'_{meas} is computed with the observation model (i.e., the inverse of equations 9 and 10), resulting in:

$$Vec'_{meas} = \begin{bmatrix} x_{meas} \\ y_{meas} \\ z_{meas} \end{bmatrix} = \begin{bmatrix} cos(\varphi)cos(\theta) \\ cos(\varphi)sin(\theta) \\ sin(\varphi) \end{bmatrix}. \tag{11}$$

The zero mean Gaussian noise η_b is modeled as $\mathcal{N}(0_{2\times1}, M_\eta)$, being M_η the result of:

$$M_\eta = J_u * J_v * M_\sigma * J_v^T * J_u^T, \tag{12}$$

where J_u and J_v correspond respectively to the jacobians of the normalized unit vector and the vector itself. The normalized vector jacobian J_u is computed by the GTSAM library [5] when applying the function Unit3, and represents the Jacobian matrix over the conversion of a vector to a unit vector. This Jacobian J_u is the result of the multiplication of the basis of the direction of the vector, matrix B, times the Jacobian of the normalization J_{norm}:

$$J_u = J\left(\frac{V}{|V|}\right) = B^T * J_{norm}. \tag{13}$$

There are three possible results for B depending on the vector's axis of rotation. Given vector $V = (a, b, c)$ to be converted into an unit vector, the three possibilities are:

$$B_{(1,0,0)} = \begin{bmatrix} 0 & c & -b \\ -b^2-c^2 & ab & ac \end{bmatrix} \tag{14}$$

if the axis is x,

$$B_{(0,1,0)} = \begin{bmatrix} -c & 0 & a \\ ab & -a^2-c^2 & bc \end{bmatrix} \tag{15}$$

if it is y, and

$$B_{(0,0,1)} = \begin{bmatrix} b & -a & 0 \\ ac & bc & -a^2-b^2 \end{bmatrix} \tag{16}$$

if it is z. The Jacobian of the normalization J_{norm} is computed as:

$$J_{norm} = \begin{bmatrix} b^2+c^2 & -ab & -ac \\ -ab & a^2+c^2 & -bc \\ -ac & -bc & a^2+b^2 \end{bmatrix} * \frac{1}{\sqrt{a^2+b^2+c^2}}. \tag{17}$$

The measured vector Jacobian J_v is:

$$J_v = \begin{bmatrix} -sin(\varphi)cos(\theta) & -cos(\varphi)sin(\theta) \\ -sin(\varphi)sin(\theta) & cos(\varphi)cos(\theta) \\ cos(\varphi) & 0 \end{bmatrix}, \tag{18}$$

and M_σ is a diagonal matrix with the associated error of each angle, σ_a and σ_e:

$$M_\sigma = \begin{bmatrix} \sigma_e^2 & 0 \\ 0 & \sigma_a^2 \end{bmatrix}. \tag{19}$$

Similarly, as the range factor, both σ_a and σ_e were adjusted in previous tests in shallow waters using the modem's datasheet information as the base and can be checked in Table I at the end of this Section. Then, the measurement vector is $Vec_{meas} = Vec'_{meas} + \eta_{bm}$.

On the other hand, the vector Vec_{est} used for the expectancy model of the bearing information $h(x)_b$ is computed using the transformation from the HF USBL pose to the estimated landmark position. The vector is computed as the distance between the HF USBL and the landmark estimated position after transforming the landmark into the HF USBL reference frame:

$${}^uP_l = {}^r T_u^{-1} \oplus^w T_r^{-1} \oplus^w P_l, \tag{20}$$

and then it is normalized to an unitary vector by using the function Unit3 vector from the GTSAM library [5] which computes it as:

$$h(x)_b = \frac{{}^uP_l}{|{}^uP_l|}. \tag{21}$$

After obtaining $h(x)_b$, the Gaussian noise model is computed with the same process as in the measurement vector (Eq. 12–19). Then Vec_{est} is the combination of $h(x)_b$ and η_{be}.

Finally, the factor is calculated as:

$$\psi(rp_j, l_k)_b = \| Vec_{est} - Vec_{meas} \|^2_\Sigma. \tag{22}$$

Bearing factors also apply the initialization algorithm 1, although they do not suffer from the same increases in uncertainty as the range factor since these factors are more informative. For reference, the range-based graph SLAM needs at least four measurements gathered in points that are not in the same plane [41] to compute the position of the landmark. Instead, in this case, the minimum number of bearing measures needed is 2, although to reduce uncertainty in the main graph the minimum number is set to 3.

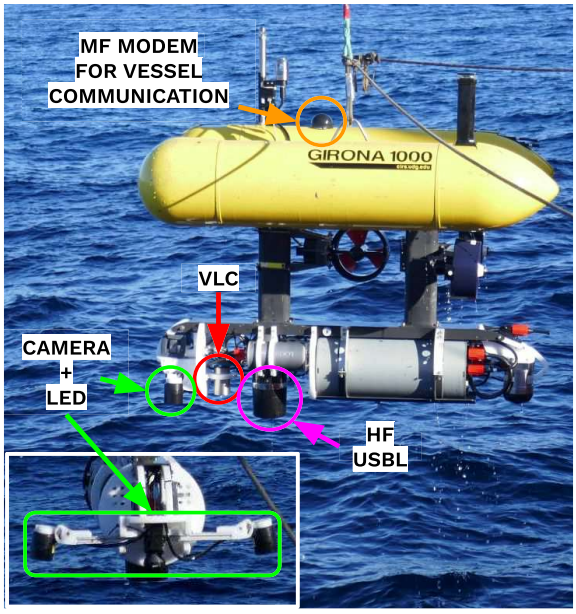

Fig. 6. AUV's extra payload for the experiments. The HF USBL is replaced by the localization MF modem when needed for the range measurements.

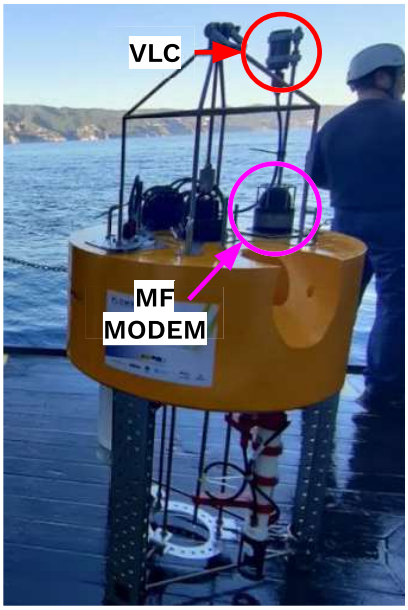

Fig. 7. Lander 1 equipped with a VLC and a MF modem.

IV. Experimental Results

A. Setup

The field experiments were carried out using a Girona 1000 [42], a multihull and reconfigurable AUV equipped with sensors for basic navigation and security. As for the inertial sensors, the AUV is equipped with a Phins Compact C3 inertial navigation system (INS) (iXblue [43]), which is used both as an IMU for the dead-reckoning part of the graph-based navigation and as ground-truth; with a DVL1000-4000m (Nortek [44]) for the linear velocity; and a miniSVS1000 (Valeport Ltd [45]) that provides water pressure and sound velocity. Apart, absolute positions are provided either with a GNSS L86 (Quectel [46]) when on the surface, or with an acoustic MF modem that communicates with the surface vessel's USBL when the AUV is underwater. In addition, for this application a specific payload was installed (Fig. 6), which was comprised by the following sensors: an optical modem based on visual light communication (VLC) (Hydromea [47]) for high-bandwidth bidirectional communication with the lander; a high-definition camera and lights for visual transects and visual mapping; and the acoustic receptors, a MF modem (18/34 kHz) (Evologics [48]) for the range-based graph SLAM or a HF USBL (42/65 kHz) (Evologics) for the bearing-based graph SLAM. When the AUV executes a range-based localization it is equipped with two different MF modems. The MF modem used for surface monitoring and USBL updates is attached at the top of the AUV for better communication with the surface vessel. Instead, the one used for localization is placed at the bottom of the AUV and pointing towards the seabed, configured to communicate with the landers. To prevent acoustic security and location signals from both modems to interfere between them, time multiplexing is applied. Therefore, each signal has its slot of time where it can send or receive data. There are three different slots: security communication AUV to Vessel (3s), USBL positioning Vessel to AUV (3s), and acoustic localization AUV to landers (4s).

Apart from the AUV, other equipment was used, such as the landers and stand-alone acoustic modems. Landers are benthic multiparametric platforms deployed at the MPAs and used to gather data to study the area during long periods [49] (Fig. 7). They are equipped with sensors capable of providing environmental data such as water temperature and pressure, photosynthetic active radiation or Chlorophyll concentration, among others, and visual data with a stereo camera [50]. In the experiments, two landers were deployed, both equipped with MF modems to communicate with each other and with a surface buoy, apart from providing range information to the AUV. The AUV's localization MF modem communicates with the landers' modems by sending and receiving acknowledgment signals, which transmit both the time of sending and the lander's identification number. Then, the algorithm computes the range by using the sending time stamp and the arrival time stamp and considering the sound speed constant. Additionally, one of the two landers was equipped with an optical modem to perform the data transmission operation with the one installed in the AUV.

For the bearing-based experiments, we deployed an HF modem (42/65 kHz) (Evologics) to emulate the acoustic tags typically used for fauna tracking. Also, since we do not know when we will receive signals from this beacon, using high frequency avoids interference with the AUV's medium frequency security signal.

The initial experiments were done outside a harbor on the coast of Catalonia (north-east of Spain), during July of 2023. Then, final results were obtained during the campaign BITER-2 on board the Sarmiento de Gamboa ship, an oceanographic research vessel from Centro Superior de Investigaciones Científicas (CSIC), which took place in different locations along the catalan coast during December 2023.

B. Experiments Design

As explained in the introduction, this work has been developed in the context of two projects: PLOME project and BITER-AUV project. Each project has its own requirements when it refers to the tasks the AUV has to accomplish. Next, we present the specifics needed for each project and what was tested during the experiments.

1) Plome Project: The objective of the PLOME project is to monitor MPAs by using easy-to-deploy and low-impact seafloor stations and AUVs. By using the seafloor stations as landmark References, the AUV navigates the area collecting information, and expanding the area to monitor further from the stations. The information is gathered by performing visual transects once the AUV is localized with respect to the stations, thus allowing repeatability of the operations. Since the data obtained by the transects is too heavy to be transmitted acoustically to the surface vessel by the AUV, this information is transmitted to the lander via optical transmission so the AUV can continue gathering more data while the lander sends small files to the surface. Alternatively, the lander can transmit larger files from its information gathering to the AUV so it carries them to the surface, acting as a "data mule". These experiments consisted of the validation of the range-based graph SLAM plus the test of PLOME project's system as a whole, which comprised:

1) Localization of the seafloor landers via range-based graph SLAM.
2) Visual transect using a convolutional neural network (CNN) trained to detect area-specific fauna [51], such as Nephrops Norvegicus or other animals.
3) Transmission/reception of data (e.g., images with detected animals or navigation data files) using the optical modem to/from the lander.

Two landers were deployed at 70 meters deep, approximately 200 meters from each other. Only one of the landers (Lander 1) was equipped with an optical modem (VLC) for data transmission. Based on the project requirements, we prepared a mission that tested all the parts in one trajectory. This complete mission begins with a circular trajectory around Lander 2 to localize it; after 2/3 of the circle, the AUV starts a visual transect to gather data between the landers in a straight line at 2 meters from the sea floor. Once it arrives near Lander 1, it navigates again in a circular trajectory until the estimated position of this lander is accurate enough. Then, the AUV automatically moves to the estimated position of the lander, and transmits data via optical communication. After the transmission finishes, the AUV resurfaces at a pre-established point.

2) Biter-Auv Project: As previously stated, the objective of the BITER-AUV project is to localize and track tagged fauna in an MPA. The AUV has to be able to localize the animals during a coverage trajectory and perform a visual mapping above their estimated position. Apart from the bearing information, the signal will also provide the identification number of the acoustic tag. Since the project is still in development [52], an Evologics HF modem was used as a substitute for the tagged animals to test the localization algorithm in a real scenario. This modem was mounted in a metallic structure, see Figure 19, for easier deployment and recovery. Similarly to the PLOME project experiments, the deployment of the HF modem was also at 70 meters depth.

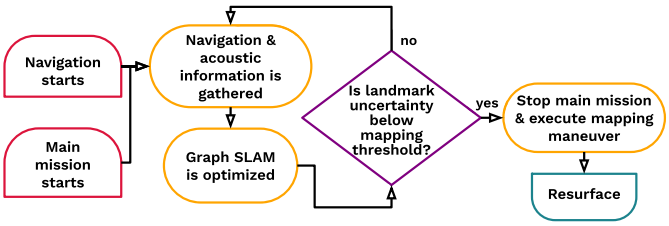

Fig. 8. General mission execution process.

TABLE II
THRESHOLDS AND OTHER PARAMETERS

Description	Value
Initialization threshold	100 m^2
Mapping threshold	25 m^2
Transmission threshold	4 m^2
USBL distance rejection	30 m
USBL time rejection	10.5 s
Inertial factor update rate	5 s

3) Mapping Algorithm: The mapping algorithm function is added to stop the current trajectory of the AUV and automatically perform a maneuver above a target. This algorithm is applied to visually map an acoustic landmark located during the bearing-based graph SLAM or to navigate the AUV above a lander and maintain a stationary position during the data transmission in the case of the range-based graph SLAM. The algorithm uses the covariance matrix trace of the estimated landmark position to interrupt the trajectory of the AUV. So, once the sum of the diagonal of that matrix is below a given threshold, the algorithm stores the estimated position and sends an interruption query to the mission control system that starts the mapping maneuver. Figure 8 presents the execution process of the mapping algorithm in combination with the whole system.

The visual mapping consists of a lawnmower trajectory with the target at the center of it. The lawnmower trajectory shape is pre-adjusted by indicating the number of sections and their respective distances before the mission starts. After it finishes, it saves the landmark id to be discarded for future mappings during the same mission.

Thresholds can be checked in Table II, with the mapping threshold being the one applied to start the visual mapping on a target and the one called transmission threshold for the automatic optical transmission with the lander maneuver. Since the visual mapping does not need the estimated position to be as precise as the transmission one, the threshold is set higher. This way, the mapping maneuver triggers earlier, saving time in the coverage mission. Because the covariance matrix provides the estimation's uncertainty, and in the case of these landmark estimates, the units are meters, the thresholds that use the trace of the covariance matrix as a measurement have m^2 as their units. These values are also dependent on the noise added to the acoustic factor. If we set a low noise

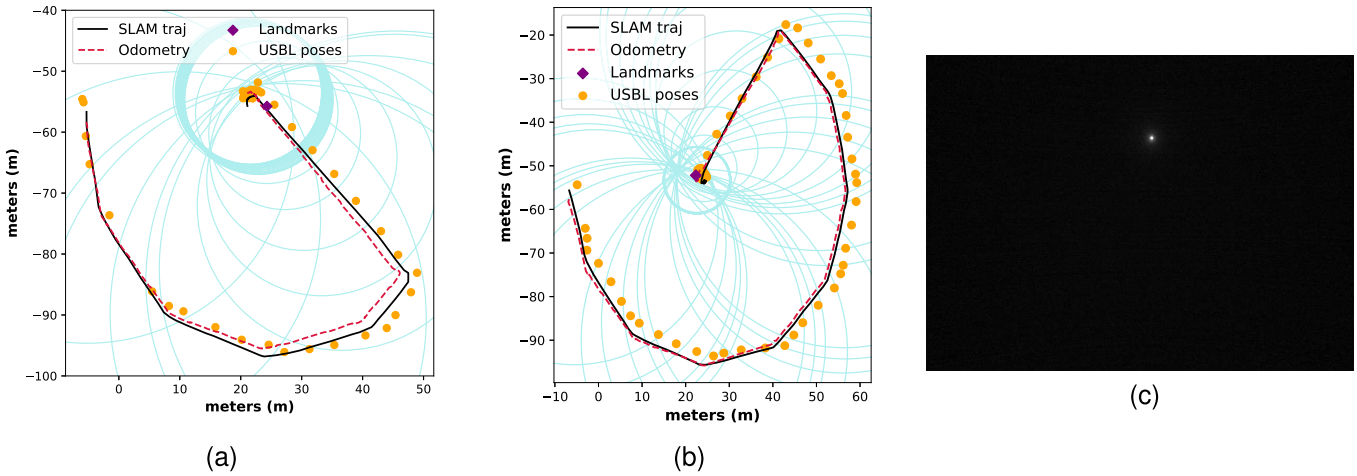

Fig. 9. Tests for the optical transmission. From left to right: (a) Transmission threshold at 10 m^2 and AUV at 12 m above seafloor during the transmission; (b) Transmission threshold at 4 m^2 and AUV at 8 m above seafloor during the transmission; (c) Image taken during the optical transmission with the lander.

value, the uncertainty, in general, will be lower; however, this could lead to problems in the entire AUV navigation if the measurements are not as accurate as expected. Instead, by adding more noise, the landmarks uncertainty will present higher values, but the optimization of the graph SLAM will be more stable. Then, we set the thresholds by taking into account the noise selected for these factors. Additionally, as stated before, we considered the minimum amount of uncertainty possible to perform such maneuvers correctly. For example, the transmission threshold is set to 4 m^2 since with an overall error of 2 m from the desired pose, the AUV could transmit the data. Then, to refine the thresholds, we tested different values during the experiments, as can be checked in Figure 9.

C. Results

1) Range-Based Graph SLAM: Since the range-based SLAM had previously been tested alone using simplified versions of the landers in shallow waters, the effort was put mainly into the combination of the different steps of the mission for the PLOME project. Before performing a whole mission, the initial experiments consisted of planned trajectories around the landers to test the different parts of the mission separately. First, we tested the localization of both landers plus the visual transect between them (Fig. 10). This way, we checked that the altitude during the transect was appropriate for the correct visual detection of fauna and that the acoustic communication was correctly configured. Two factors influence the shape of the trajectory: the tasks to be performed for the PLOME project previously detailed (the visual transect and the localization of both landers), and the landmarks position's observability. In the case of range-based localization, the optimal trajectory shape to estimate the position of an acoustic beacon is a circular one around the landmark based on the observability of the system as demonstrated in [53]. The variations in depth during the trajectory (see Figure 11) were included in all trajectories to increase the observability in the z-axis. The ranges received

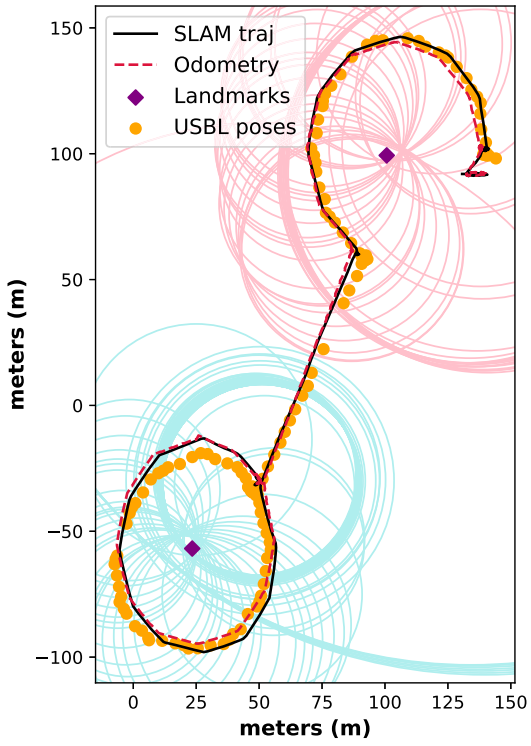

Fig. 10. Preliminary range-based graph SLAM experiment with landmark localization and visual transect.

from each lander are also presented in the 2D figures 10, 9, and 12 (in light blue for Lander 1 and pink for Lander 2).

The next step was to test different parameters for the optical transmission, such as the transmission threshold and the altitude above the lander for the transmission. The threshold was calibrated so it assures a correct transmission and also so it shortens the trajectory. These tests consisted of a circular trajectory around Lander 1. Figure 9 shows two tests with different parameter combinations.

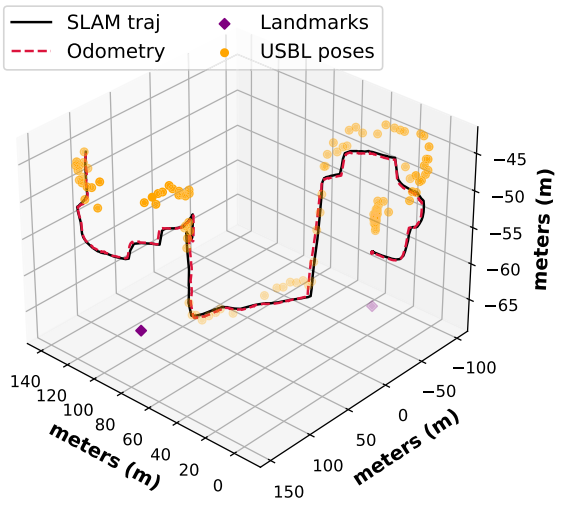

Fig. 11. PLOME project full mission (3D view).

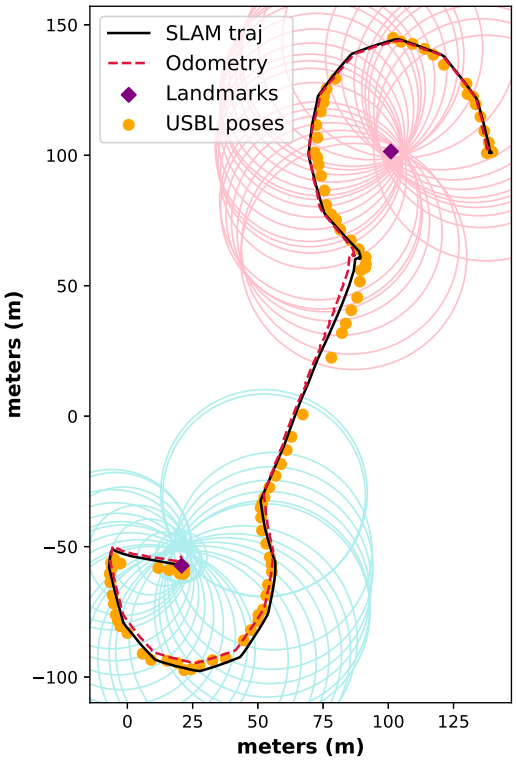

Fig. 12. PLOME project full mission (Top view).

TABLE III
FINAL COVARIANCE TRACES IN THE RANGE-BASED EXPERIMENTS

Experiment figure	Lander nº	Covariance trace
10	2	2.55 m^2
10	1	3.71 m^2
9a	1	6.49 m^2
9b	1	1.61 m^2
11 & 12	2	2.43 m^2
11 & 12	1	1.94 m^2

Finally, figures 11 and 12 present the complete navigation of the AUV computed by the range-based graph SLAM in 3D and 2D with all the steps of the PLOME project. For this final test, the transmission threshold was set to 4 m^2, and we were able to transmit several navigation data files and some images gathered in the visual transect between the two landers, selected by the automatic detection algorithm, during a transmission of 10 minutes. Figure 13 and Table III show the covariance trace of each landmark estimation in the experiments done with range-based SLAM. This values reflect the uncertainty in the estimation of each landmark. In Figure 13 the evolution of the landmarks' uncertainties is shown for the two main experiments, and includes the transmission threshold (4 m^2). Table III presents these uncertainties for all range-based tests at the moment the experiment finishes.

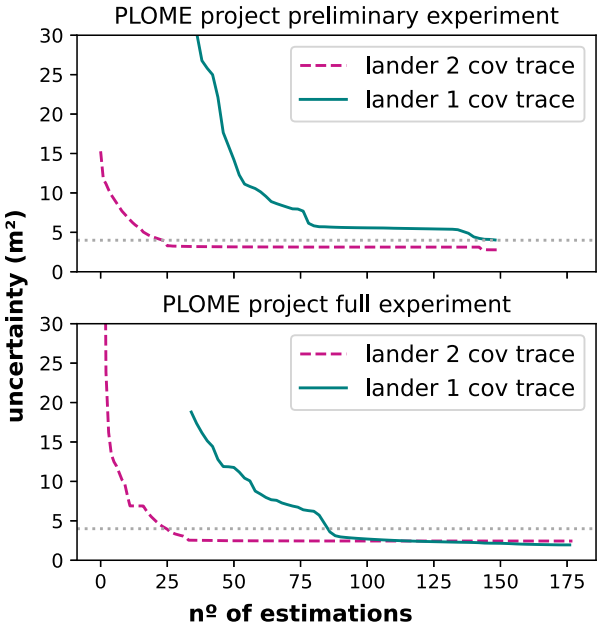

Fig. 13. Evolution of the landmarks' uncertainties during the range-based experiments.

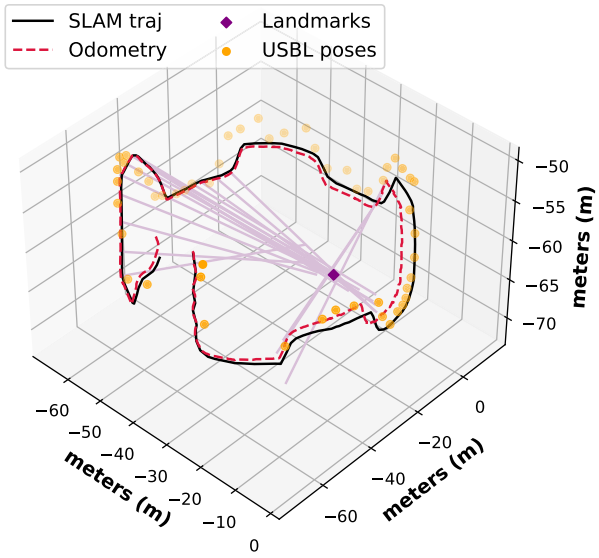

Fig. 14. Initial test with bearing-based graph SLAM.

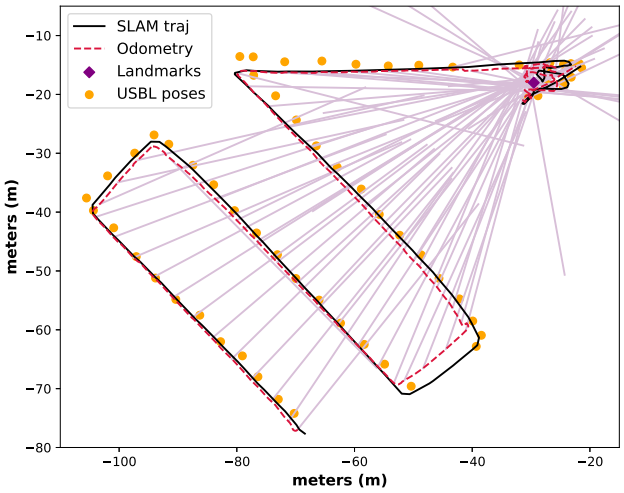

Fig. 15. Initial bearing-based graph SLAM coverage experiment (Top view) with mapping threshold at 50 m^2 and smaller mapping maneuver.

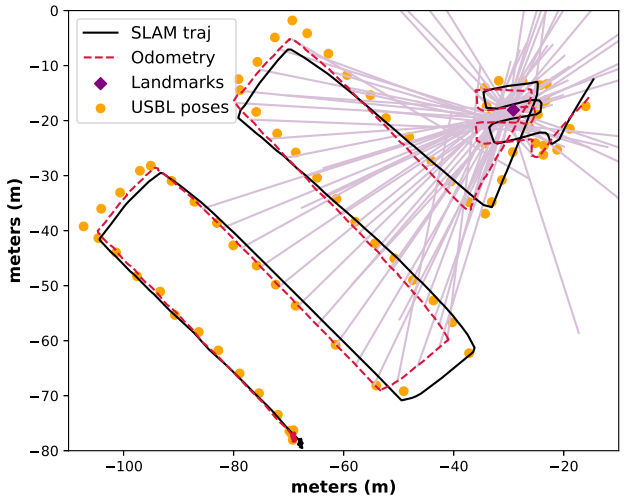

Fig. 17. Second bearing-based graph SLAM coverage experiment (Top view) with mapping threshold at 25 m^2 and bigger mapping maneuver.

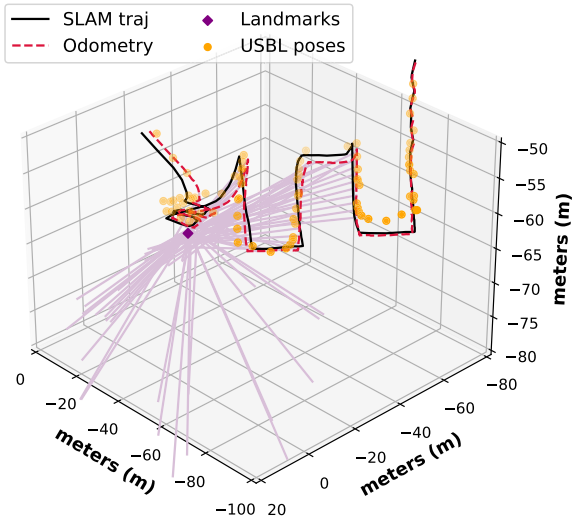

Fig. 16. Second bearing-based graph SLAM coverage experiment (3D view) with mapping threshold at 25 m^2 and bigger mapping maneuver.

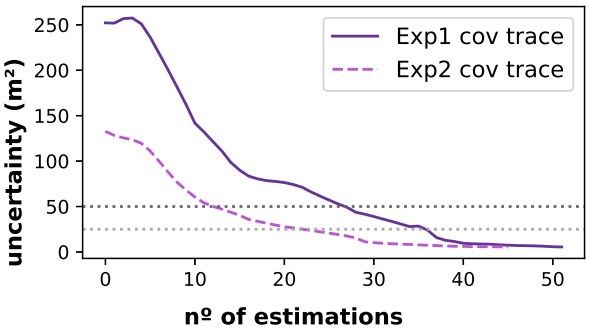

Fig. 18. Evolution of the beacon's uncertainty during the two BITER-AUV project experiments.

TABLE IV
FINAL COVARIANCE TRACES IN THE BEARING-BASED EXPERIMENTS

Experiment figure	Covariance trace
14	35.60 m^2
15	6.66 m^2
16 & 17	5.49 m^2

2) Bearing-Based Graph SLAM: As for the bearing-based graph SLAM, the results are shown in Figures 14, 15, 16 and 17. Similarly to the range-based SLAM results, these figures show the navigation computed by the graph SLAM, the odometry, the USBL poses, and the estimated landmark position. The lines drawn in light purple represent the bearings received by the AUV from the HF modem. Since the acoustic signal does not provide the range, all the bearings are drawn with the same length of 50 m. In the first experiment, the AUV did a circular maneuver around the modem position (Fig. 14), which we knew due to the deployment information. After the initial test, we prepared a lawnmower coverage mission simulating the search of tagged animals in an area. We were able to test several times this coverage mission and two experiments are shown in Figures 15, 16 and 17.

The AUV starts with a fixed lawnmower trajectory, and once the landmark estimation uncertainty is low enough, it triggers the visual mapping above that estimated position. After that, the AUV returns to the surface. Figure 15 presents an experiment with a mapping threshold of 50 m^2 and a mapping maneuver with small distances. Then, figures 16 and 17 present another experiment with a lower mapping threshold of 25 m^2 and a more extensive mapping maneuver. Also, Figure 14 and 16 show how, as in the range-based experiments, in this missions the elevation changes during the trajectories to increase the observability of the acoustic landmark in the z-axis. Figure 18 and Table IV present the covariance trace of the landmark's estimation in these bearing-based SLAM experiments. Similar to the range-based case, Figure 18 shows how the beacon's uncertainty decreases as the beacon signals are received and the graph SLAM is optimized. Both experiment results are shown in the same graphic plus the

Fig. 19. HF modem mapped during the bearing-based graph SLAM experiments.

two mapping thresholds used for the experiments, 50 m^2 for experiment 1 (Fig. 15), and 25 m^2 for experiment 2 (Fig. 17).

Finally, Figure 19 presents a frame from the visual mapping performed in this experiment, which shows the HF modem and the metallic structure for deployment.

V. Discussion

Overall, the experimental results were successful since the acoustic localization applying graph SLAM with either ranges or bearings was accurate enough to transmit data to the lander and map the HF modem.

Our simplified method for the USBL position factor integration worked correctly by creating the nodes and updating them a posteriori once the USBL information was received. Besides this, a minor improvement to the outlier distance rejection should be applied, changing how it computes the distance from Euler, the current implementation, to Mahalanobis.

In the case of the range-based graph SLAM, the 2d figures with the ranges drawn (Figures 9, 10, and 12) seem that sometimes the ranges do not coincide all in the same spot. That is because the range can be considered spherical and depends also on the altitude difference of the AUV to the lander. This is why when the AUV is above the lander transmitting data, there are many concentric circles around it. In the two tests presented in Fig. 9, the concentric circles show at which distance the AUV was above the lander, approximately 11 meters in Fig. 9a, and around 7 meters in Fig. 9b. In terms of accuracy in the estimation, Table III covariance traces show how by acquiring signals with a circular trajectory around the lander, we can achieve very low values of uncertainty, like the case of experiments in Figures 9b and 12. Also, by setting the threshold to a lower value, the AUV takes more time to trigger the transmission maneuver, but the transmission position is more accurate, as can be checked in Figure 9 and the covariance traces of these experiments. The evolution of the uncertainty in Figure 13 shows how, once the landmark has been initialized in the graph SLAM, the algorithm needs at least 25 more measurements to estimate the position of the landmark within an uncertainty of 4 m^2. A low uncertainty in the landmark estimation also means low uncertainty in the estimated pose of the AUV since they are correlated.

As for the bearing-based graph SLAM, we had some problems due to the position of the HF modem in the metallic structure, which resulted in that depending on the AUV's position, it could not receive any acoustic signals. Figure 14 shows how only in certain parts of the circular trajectory signals were received. Taking this restriction into account, we prepared the coverage missions in the zone where the AUV could hear the HF modem to be able to simulate a coverage and mapping mission in a real scenario. Aside from that, another issue is the deviation of some bearings when received while the AUV was turning. This issue arises from the difference in orientation of the AUV from when it receives the signal to the processing of this information and inclusion in the graph. If the AUV is turning too fast and receives a bearing signal, it can provoke that the bearing does not point to the landmark. For example, in the coverage part of Figure 17, the three bearing deviations correspond to the robot turning 90°. Then, a filter with the AUV's angular velocity should be implemented to discard the bearing information if the robot's angular velocity surpasses a threshold in order to avoid this problem.

The estimation accuracy in the bearing-based SLAM presents higher values than the range-based ones. Several factors could influence this, such as the lack of measurements in the case of Figure 14, the fact we did not use observability-optimized trajectories instead of a classical coverage lawnmower trajectory, and as previously stated in the Experimental Design section, that the minimum uncertainty achievable depends on the noise set for the acoustic factor. The range-based localization presents lower uncertainty values since the noise set is lower in proportion to the bearing-based localization. In terms of performance, the amount of measurements needed to reach the mapping threshold is between 20 and 30. Experiment 2's case shows how, despite starting to receive signals further in the trajectory, it passes both thresholds faster than in Experiment 1. This difference could be that by acquiring measurements in closer proximity and thus having more distance in angle between measurements, it needed fewer signals, for they provided more information. Nevertheless, the AUV visually mapped the tracked beacon in both coverage experiments.

VI. Conclusion and Future Work

This article presents the implementation of a modular acoustic graph SLAM algorithm that can be adapted to measures of either ranges or bearings to estimate the positions of acoustic landmarks in underwater scenarios. We implemented novel methods in our acoustic graph SLAM algorithm, such as a simplification for the integration of USBL position factor considering the transmission delay, an initialization method for range and bearing factors to reduce the uncertainty in the graph SLAM, and the creation of a 3D bearing factor which combines the two angles provided by the acoustic signal (azimuth and elevation). As the results show, our acoustic localization algorithm proves to be accurate enough to perform tasks successfully once it has localized the acoustic beacons. Moreover, the outputs of this work can be used in many other applications, especially ones that require precise underwater

localization, such as mapping the seabed, interaction or manipulation with underwater elements, or navigating through a large area without increasing the uncertainty too much. Thanks to its modularity, the factors presented here and their respective integration methods can be implemented in combination with other sensor information in a graph SLAM framework for any application that can benefit from acoustic information. The next step in this work is the implementation of path planning strategies that consider acoustic information to optimize the AUV navigation while tracking acoustic beacons in an unexplored large area.

REFERENCES

[1] (2019). *Classify 30% of the National Maritime Space As Marine Protected Areas (MPAS) By 2030*. [Online]. Available: https://sdgs.un.org/partnerships/classify-30-national-maritime-space-marine-protected-areas-mpas-2030#deliverables

[2] (2023). *Marine Protected Areas in Europe's Seas*. Accessed: Apr. 28, 2025. [Online]. Available: https://www.eea.europa.eu/en/analysis/indicators/marine-protected-areas-in-europes-seas

[3] M. C. Pérez et al., "Marine ecosystems observation by a cooperative auv in the plome project," *Instrum. Viewpoint*, no. 22, p. 84, 2023.

[4] I. Masmitja et al., "Mobile robotic platforms for the acoustic tracking of deep-sea demersal fishery resources," *Sci. Robot.*, vol. 5, no. 48, p. 3701, Nov. 2020.

[5] F. Dellaert, "Factor graphs and gtsam: A hands-on introduction," Georgia Institute of Technology, Atlanta, GA, USA, Tech. Rep. GT-RIM-CP&R-2012-002, 2012.

[6] M. Kaess, H. Johannsson, R. Roberts, V. Ila, J. Leonard, and F. Dellaert, "ISAM2: Incremental smoothing and mapping with fluid relinearization and incremental variable reordering," in *Proc. IEEE Int. Conf. Robot. Autom.*, May 2011, pp. 3281–3288.

[7] M. Real, P. Vial, N. Palomeras, and M. Carreras, "Underwater acoustic localization using pose-graph SLAM," in *Proc. OCEANS*, Jun. 2023, pp. 1–6.

[8] D. Heckman and R. Abbott, "An acoustic navigation technique," in *Proc. IEEE Int. Conf. Eng. Ocean Environ.*, Jan. 1973, pp. 591–595.

[9] M. Watson, J. Berkowitz, and M. Wapner, "Ultra-short baseline acoustic tracking system," in *Proc. OCEANS*, 1983, pp. 214–218.

[10] P. Corke, C. Detweiler, M. Dunbabin, M. Hamilton, D. Rus, and I. Vasilescu, "Experiments with underwater robot localization and tracking," in *Proc. IEEE Int. Conf. Robot. Autom.*, Apr. 2007, pp. 4556–4561.

[11] M. Yuan, Y. Li, Y. Li, S. Pang, and J. Zhang, "A fast way of single-beacon localization for AUVs," *Appl. Ocean Res.*, vol. 119, Feb. 2022, Art. no. 103037. [Online]. Available: https://www.sciencedirect.com/science/article/pii/S0141118721004946

[12] B. Allotta et al., "An imu and usbl-aided buoy for underwater localization," in *Proc. 8th Int. Conf. Comput. Methods Mar. Eng. (MARINE)*, 2017, pp. 449–460.

[13] P. Newman and J. Leonard, "Pure range-only sub-sea SLAM," in *Proc. IEEE Int. Conf. Robot. Autom.*, Sep. 2003, pp. 1921–1926.

[14] R. M. Eustice, H. Singh, and L. L. Whitcomb, "Synchronous-clock, one-way-travel-time acoustic navigation for underwater vehicles," *J. Field Robot.*, vol. 28, no. 1, pp. 121–136, Jan. 2011. [Online]. Available: https://onlinelibrary.wiley.com/doi/abs/10.1002/rob.20365

[15] Y. Guo, X. Kang, Q. Han, and J. Wang, "A localization algorithm for underwater wireless sensor networks based on ranging correction and inertial coordination," *KSII Trans. Internet Inf. Syst. (TIIS)*, vol. 13, no. 10, pp. 4971–4987, 2019.

[16] S. Poursheikhali and H. Zamiri-Jafarian, "TDOA based target localization in inhomogenous underwater wireless sensor network," in *Proc. 5th Int. Conf. Comput. Knowl. Eng. (ICCKE)*, Oct. 2015, pp. 1–6.

[17] P. Mendes and P. Batista, "A study on cooperative navigation of AUVs based on bearing measurements," in *Proc. OCEANS*, Sep. 2021, pp. 1–8.

[18] Y. Sekimori, T. Matsuda, and T. Maki, "Bearing-only aided bearing, elevation, depth difference self-localization for multiple AUVs," in *Proc. OCEANS*, Feb. 2022, pp. 1–6.

[19] R. Costanzi, D. Fenucci, V. Manzari, and A. Caiti, "Bearing-only AUV tracking performance: The effect of uncertainty in underwater nodes position," in *Proc. OCEANS MTS/IEEE Monterey*, Sep. 2016, pp. 1–6.

[20] N. Modalavalasa, G. S. B. Rao, K. S. Prasad, L. Ganesh, and M. N. V. S. S. Kumar, "A new method of target tracking by EKF using bearing and elevation measurements for underwater environment," *Robot. Auto. Syst.*, vol. 74, pp. 221–228, Dec. 2015. [Online]. Available: https://www.sciencedirect.com/science/article/pii/S0921889015001633

[21] S. Yun, Y. Kim, B. Lee, and S. Sung, "A normalized measurement vector model for enhancing localization performance of 6-DoF bearing-only SLAM," *Int. J. Control, Autom. Syst.*, vol. 16, no. 2, pp. 912–920, Apr. 2018.

[22] T. Lemaire, S. Lacroix, and J. Sola, "A practical 3D bearing-only SLAM algorithm," in *Proc. IEEE/RSJ Int. Conf. Intell. Robots Syst.*, Aug. 2005, pp. 2449–2454.

[23] C. M. Clark et al., "Tracking and following a tagged leopard shark with an autonomous underwater vehicle," *J. Field Robot.*, vol. 30, no. 3, pp. 309–322, May 2013. [Online]. Available: https://onlinelibrary.wiley.com/doi/abs/10.1002/rob.21450

[24] T. Maki, T. Matsuda, T. Sakamaki, T. Ura, and J. Kojima, "Navigation method for underwater vehicles based on mutual acoustical positioning with a single seafloor station," *IEEE J. Ocean. Eng.*, vol. 38, no. 1, pp. 167–177, Jan. 2013.

[25] R. Smith, M. Self, and P. Cheeseman, "Estimating uncertain spatial relationships in robotics," in *Proc. IEEE Int. Conf. Robot. Automat.*, Raleigh, NC, USA, 1987, p. 850. [Online]. Available: http://dx.doi.org/10.1109/ROBOT.1987.1087846

[26] S. Thrun, "Particle filters in robotics," in *UAI*, 2002, pp. 511–518.

[27] S. J. Julier and J. K. Uhlmann, "A counter example to the theory of simultaneous localization and map building," in *Proc. ICRA IEEE Int. Conf. Robot. Autom.*, May 2001, pp. 4238–4243.

[28] F. Dellaert and M. Kaess, "Factor graphs for robot perception," *Found. Trends Robot.*, vol. 6, nos. 1–2, pp. 1–139, 2017.

[29] M. Kaess, A. Ranganathan, and F. Dellaert, "ISAM: Incremental smoothing and mapping," *IEEE Trans. Robot.*, vol. 24, no. 6, pp. 1365–1378, Dec. 2008.

[30] S. Chaves, E. Galceran, P. Ozog, J. Walls, and R. Eustice, "Pose-graph SLAM for underwater navigation," 2017. [Online]. Available: http://dx.doi.org/10.1007/978-3-319-55372-6_7

[31] M. Holder, S. Hellwig, and H. Winner, "Real-time pose graph SLAM based on radar," in *Proc. IEEE Intell. Vehicles Symp. (IV)*, Jun. 2019, pp. 1145–1151.

[32] R. Worley et al., "Robot localization in water pipes using acoustic signals and pose graph optimization," *Sensors*, vol. 20, no. 19, p. 5584, Sep. 2020. [Online]. Available: https://www.mdpi.com/1424-8220/20/19/5584

[33] A. Moura, J. Antunes, A. Dias, A. Martins, and J. Almeida, "Graph-SLAM approach for indoor UAV localization in warehouse logistics applications," in *Proc. IEEE Int. Conf. Auton. Robot Syst. Competitions (ICARSC)*, Apr. 2021, pp. 4–11.

[34] M. Franchi et al., "Maximum a Posteriori estimation for AUV localization with USBL measurements," *IFAC-PapersOnLine*, vol. 54, no. 16, pp. 307–313, 2021. [Online]. Available: https://www.sciencedirect.com/science/article/pii/S2405896321015111

[35] L. Zhang, L.-T. Hsu, and T. Zhang, "A novel INS/USBL integrated navigation scheme via factor graph optimization," *IEEE Trans. Veh. Technol.*, vol. 71, no. 9, pp. 9239–9249, Sep. 2022.

[36] N. Funabiki, B. Morrell, J. Nash, and A.-A. Agha-Mohammadi, "Range-aided pose-graph-based SLAM: Applications of deployable ranging beacons for unknown environment exploration," *IEEE Robot. Autom. Lett.*, vol. 6, no. 1, pp. 48–55, Jan. 2021.

[37] M. Flynn, B. W. O'Neill, D. P. Hart, and J. J. Leonard, "A comparative analysis of maneuvering strategies for cooperative range-based localization," in *Proc. OCEANS*, Jun. 2023, pp. 1–10.

[38] M. Cheng, M. R. K. Aziz, and T. Matsumoto, "Integrated factor graph algorithm for DOA-based geolocation and tracking," *IEEE Access*, vol. 8, pp. 49989–49998, 2020.

[39] P. Vial, M. Castillón, N. Palomeras, M. Carreras, and P. Ridao, "Inertial navigation framework for multimodal underwater graph SLAM," in *Proc. OCEANS*, Jun. 2023, pp. 1–8.

[40] C. Forster, L. Carlone, F. Dellaert, and D. Scaramuzza, "On-manifold preintegration for real-time visual-inertial odometry," *IEEE Trans. Robot.*, vol. 33, no. 1, pp. 1–21, Feb. 2017.

[41] H. Li, "Observability for 3-D range-only positioning system," in *Proc. 40th Chin. Control Conf. (CCC)*, Jul. 2021, pp. 3509–3514.

[42] D. Ribas, N. Palomeras, P. Ridao, M. Carreras, and A. Mallios, "Girona 500 AUV: From survey to intervention," *IEEE/ASME Trans. Mechatronics*, vol. 17, no. 1, pp. 46–53, Feb. 2012.

[43] (2024). *iXBlue*. [Online]. Available: https://www.ixblue.com/

[44] (2024). *Nortek*. [Online]. Available: https://www.nortekgroup.com/

[45] (2024). *Valeport*. [Online]. Available: https://www.valeport.co.uk/
[46] (2024). *Quectel*. [Online]. Available: https://www.quectel.com/
[47] (2024). *Hydromea*. [Online]. Available: https://www.hydromea.com/
[48] (2024). *EvoLogics GmbH*. [Online]. Available: https://evologics.com/
[49] D. M. Toma et al., "Multiparametric benthic landers for monitoring fishing-impacted deep-sea ecosystems," in *Proc. OCEANS*, Jun. 2023, pp. 1–5.
[50] E. Alfaro-Dufour, C. Muntaner-González, A. Martorell-Torres, and G. Oliver-Codina, "Lanty: A deep sea stereo vision system," in *Proc. IEEE Int. Conf. Ind. Technol. (ICIT)*, Mar. 2024, pp. 1–6.
[51] A. B. Burguera, F. Bonin-Font, D. Chatzievangelou, M. V. Fernandez, and J. Aguzzi, "Deep learning for detection and counting of nephrops norvegicus from underwater videos," *ICES J. Mar. Sci.*, vol. 81, no. 7, pp. 1307–1324. [Online]. Available: https://doi.org/10.1093/icesjms/fsae089
[52] G. Batet, I. Masmitja, D. Sarria, S. Gomariz, and J. D. Rio, "Engineering a testbed for bidirectional acoustic tag development," in *Proc. OCEANS*, Jun. 2023, pp. 1–6.
[53] B. T. Hinson. (2014). *Observability-Based Guidance and Sensor Placement*. [Online]. Available: https://api.semanticscholar.org/CorpusID:125532547

Marta Real received the B.S. degree in industrial electronics and automation engineering and the M.C. degree in automatic control and robotics from the Universitat Politécnica de Catalunya, in 2019 and 2022, respectively. She is currently pursuing the Ph.D. degree with the Institut ViCOROB, Universitat de Girona. Her research focuses on underwater localization, path planning, and exploration using AUVs.

Pau Vial received the B.S. degree in industrial engineering from the Universitat de Girona, Catalonia, in 2018, and the M.Sc. degree in industrial engineering from the Universitat Politécnica de Catalunya, Catalonia, in 2020. He is currently pursuing the Ph.D. degree in localization techniques for an AUV with the Institut VICOROB, Universitat de Girona. His research interests include optimization techniques, machine learning, and Lie theory applied to underwater robotic navigation. He received the Best Bachelor's Student Award from the Universitat de Girona.

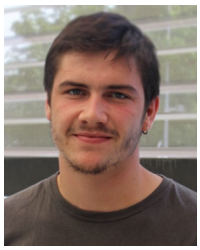

Roger Pi received the B.S. degree in computer engineering from the Universitat de Girona in 2017, the joint M.Sc. degree in computer vision and robotics from the University of Burgundy, the Universitat de Girona, and Heriot-Watt University, in 2019, and the Ph.D. degree from the Underwater Robotics Research Center (CIRS), Universitat de Girona, in 2024. His research focuses on intervention operations for autonomous underwater vehicles. He received the Best Master's Student Award.

Narcís Palomeras (Member, IEEE) received the B.Sc. degree in computer science and the Ph.D. degree in computer engineering from the Universitat de Girona, Catalonia, Spain, in 2004 and 2011, respectively. He is a Post-Doctoral Fellow with the Institut VICOROB. He has participated in several international research projects. His activity is mainly focused on underwater robotics in topics such as intelligent control architectures and mission control.

Marc Carreras (Member, IEEE) received the Ph.D. degree in industrial engineering. He was with the Underwater Robotics Laboratory, University of Girona, Spain, for more than 25 years. He has led multiple national and international research projects about AUV applications. He is the author of more than 170 publications. He has directed seven doctoral thesis and collaborated in the winning teams of several international student AUV competitions. His research topics are AUV design, navigation, mapping, machine learning, and path planning.